Journal of Controlled Release 202 (2015) 83–92

Contents lists available at ScienceDirect

Journal of Controlled Release

journal homepage: www.elsevier.com/locate/jconrel

Coating nanocarriers with hyaluronic acid facilitates intravitreal drug delivery for retinal gene therapy☆

Thomas F. Martens [a,b,*], Katrien Remaut [a], Hendrik Deschout [c], Johan F.J. Engbersen [d], Wim E. Hennink [e], Mies J. van Steenbergen [e], Jo Demeester [a], Stefaan C. De Smedt [a,*], Kevin Braeckmans [a,b,*]

[a] Laboratory of General Biochemistry and Physical Pharmacy, Faculty of Pharmaceutical Sciences, Ghent University, Ottergemsesteenweg 460, 9000 Ghent, Belgium
[b] Center for Nano-and Biophotonics (NB-Photonics), Ghent University, Ottergemsesteenweg 460, 9000 Ghent, Belgium
[c] EPFL STI IBI-STI LBEN, BM 2138 (Bâtiment BM), Station 17, CH-1015 Lausanne, Switzerland
[d] Department of Biomedical Chemistry, MIRA Institute for Biomedical Technology and Technical Medicine, Faculty of Science and Technology, University of Twente, P.O. Box 217, 7500 AE Enschede, The Netherlands
[e] Department of Pharmaceutics, Utrecht Institute for Pharmaceutical Sciences (UIPS), Utrecht University, P.O. Box 80.082, 3508 TB Utrecht, The Netherlands

ARTICLE INFO

Article history:
Received 12 September 2014
Accepted 24 January 2015
Available online 26 January 2015

Keywords:
Hyaluronic acid
Intravitreal
Retinal gene delivery
Polyplexes
Molecular weight

ABSTRACT

Retinal gene therapy could potentially affect the lives of millions of people suffering from blinding disorders. Yet, one of the major hurdles remains the delivery of therapeutic nucleic acids to the retinal target cells. Due to the different barriers that need to be overcome in case of topical or systemic administration, intravitreal injection is an attractive alternative administration route for large macromolecular therapeutics. Here it is essential that the therapeutics do not aggregate and remain mobile in the vitreous humor in order to reach the retina. In this study, we have evaluated the use of hyaluronic acid (HA) as an electrostatic coating for nonviral polymeric gene nanomedicines, p(CBA-ABOL)/pDNA complexes, to provide them with an anionic hydrophilic surface for improved intravitreal mobility. Uncoated polyplexes had a Z-averaged diameter of 108 nm and a zeta potential of +29 mV. We evaluated polyplexes coated with HA of different molecular weights (22 kDa, 137 kDa and 2700 kDa) in terms of size, surface charge and complexation efficiency and noticed their zeta potentials became anionic at 4-fold molar excess of HA-monomers compared to cationic monomers, resulting in submicron ternary polyplexes. Next, we used a previously optimized ex vivo model based on excised bovine eyes and fluorescence single particle tracking (fSPT) microscopy to evaluate mobility in intact vitreous humor. It was confirmed that HA-coated polyplexes had good mobility in bovine vitreous humor, similar to polyplexes functionalized with polyethylene glycol (PEG), except for those coated with high molecular weight HA (2700 kDa). However, contrary to PEGylated polyplexes, HA-coated polyplexes were efficiently taken up in vitro in ARPE-19 cells, despite their negative charge, indicating uptake via CD44-receptor mediated endocytosis. Furthermore, the HA-polyplexes were able to induce GFP expression in this in vitro cell line without apparent cytotoxicity, where coating with low molecular weight HA (22 kDa) was shown to induce the highest expression. Taken together our experiments show that HA-coating of nonviral gene complexes is an interesting approach towards retinal gene therapy by intravitreal administration. To our knowledge, this is the first time electrostatic HA-coating of polyplexes with different molecular weights has been evaluated in terms of their suitability for intravitreal delivery of therapeutic nucleic acids towards the retina.

1. Introduction

Gene therapy has long been recognized as a promising therapeutic avenue to effectively treat dystrophies with a genetic cause. Especially retinal gene therapy has been identified as a favored candidate, as the eye is an easily accessible organ which is shielded from systemic circulation, thus minimizing potential unwanted side-effects. Furthermore, in recent years several blinding dystrophies have been linked to genetic aberrations in the retina, such as RPE65-Leber congenital amaurosis (RPE65-LCA), Leber Hereditary Optic Neuropathy (LHON) and X-linked juvenile retinoschisis. The promise of gene therapy was substantiated in different clinical studies in patients suffering from RPE65-LCA [1–4], which further spurred research on retinal gene therapy.

To protect the therapeutic nucleic acids (NAs) from degradation during the delivery process and to aid in their transport towards the target cells, they are usually packaged into nano-sized particles. Even though most clinical successes so far have been achieved with viral vectors,

☆ This work is done in Ghent, Belgium.

* Corresponding authors at: Ghent University, Laboratory of General Biochemistry and Physical Pharmacy, Ottergemsesteenweg 460, B-9000 Ghent, Belgium. Tel.: +32 9264 8049; fax: +32 9264 8189.
E-mail addresses: Thomas.Martens@Ugent.be (T.F. Martens), Stefaan.Desmedt@Ugent.be (S.C. De Smedt), Kevin.Braeckmans@Ugent.be (K. Braeckmans).

http://dx.doi.org/10.1016/j.jconrel.2015.01.030
0168-3659/

cost and safety concerns dictate the need for cheaper and safer alternatives [5]. Nonviral vectors, such as cationic liposomes and polymers, can be designed to be biocompatible and are more easily manufactured on a large scale [6]. When combined with negatively charged NAs, they spontaneously form binary polyelectrolyte complexes (PECs) of about 100–200 nm in size, with easily adaptable surface characteristics [7]. In the case of retinal gene therapy, these NA/carrier complexes have to be delivered into the target cells in the neural retina or retinal pigment epithelium (RPE), located at the posterior part and the periphery of the eye (Fig. 1). However, the impermeability to large macromolecular compounds of the blood-retina barrier (BRB) and the corneal epithelium discourage systemic administration and topical instillation, respectively [8]. Therefore, intraocular administration routes which bypass these ocular barriers are frequently employed (Fig. 1). While clinical success has been achieved primarily by subretinal injection of nanoparticles, this procedure is known to be very invasive, potentially associated with serious adverse effects and not feasible on a large scale [9]. Therefore, intravitreal injection represents an attractive alternative route of administration, with the essential requirement that the therapeutics remain mobile in the vitreous humor in order to reach the retinal target cells. Indeed, we have previously shown that the vitreous humor poses a barrier to nanocarriers for retinal gene delivery [9,10].

Recently we reported on an ex vivo assay for measuring the mobility of fluorescent nanoparticles in intact vitreous humor on a single-particle level [9]. By removing the anterior parts (cornea, iris, and lens) of excised bovine eyes, an optical window was formed allowing us to use high-resolution fluorescence microscopy without damaging the fragile structure of the vitreous humor. This way, we were able to visualize diffusion of nanoparticles on a sub-resolution scale and analyze their behavior by using fluorescence single particle tracking (fSPT) [9]. We have shown that the mobility of gene nanomedicines in the vitreous body can be improved by shielding their cationic surface charge with a coating of polyethylene glycol (PEG). Unfortunately, PEGylation prevents successful cell transfection since the nanomedicines can no longer interact with the cell membrane and are not internalized by the target cells [11,12]. Therefore, an alternative coating strategy is needed that combines excellent nanoparticle mobility in the vitreous humor with efficient cell uptake and transfection.

In the present study we have evaluated hyaluronic acid (HA) for this purpose. HA is an anionic biodegradable, non-immunogenic biopolymer which is ubiquitously present in mammalian organisms (Fig. 2A). It is a nonsulfated glycosaminoglycan, composed of alternating disaccharide units of N-acetyl-D-glucosamine and D-glucuronic acid, linked by alternating β-1,4 glycosidic and β-1,3 glucuronidic bonds [13]. Given its well-tolerated and biocompatible nature, HA has gained a lot of interest in the field of drug delivery [13]. HA was postulated as a cryoprotectant in the formulation of liposomal drug delivery vectors [14] and as a means of evading the complement system after intravenous injection [15,16]. Furthermore, it was used for targeting CD44-overexpressing tumor tissues [16–19], since it is known that HA is a ligand for receptors such as CD44, RHAMM, LYVE-1, etc. [13]. HA might be an interesting molecule for ocular delivery as well since it is a major constituent of the vitreous humor [20], is found throughout the retina [21] and many retinal cell types have been shown to express CD44-receptors on their surface [22,23].

Here, we investigated the use of HA with different molecular weights (MWs) (22 kDa, 137 kDa, 2700 kDa) as an electrostatic coating of cationic polymeric pDNA gene complexes. These nonviral

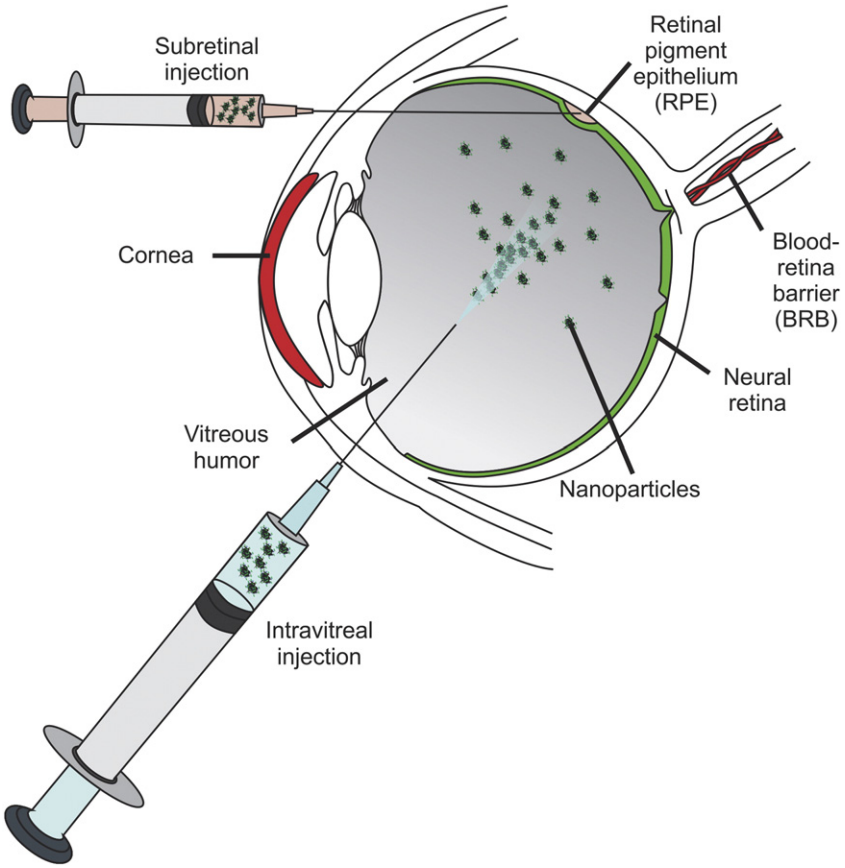

Fig. 1. Schematic illustration of different intra-ocular administration routes. Systemic and topical delivery of gene nanomedicines to the retina (shown in green) is hampered by different ocular barriers, such as the blood-retina barrier and the cornea, respectively (shown in red). Intra-ocular injections are used as an effective way to bypass these barriers. The upper syringe shows a subretinal injection, where the cargo is delivered in the subretinal space, between the neural retina and the RPE cell layer. The lower syringe shows an intravitreal injection, where the therapeutics are injected in the vitreous humor (central gray part). After intravitreal injection, the cargo has to migrate to the retinal target cells in the posterior part of the eye.

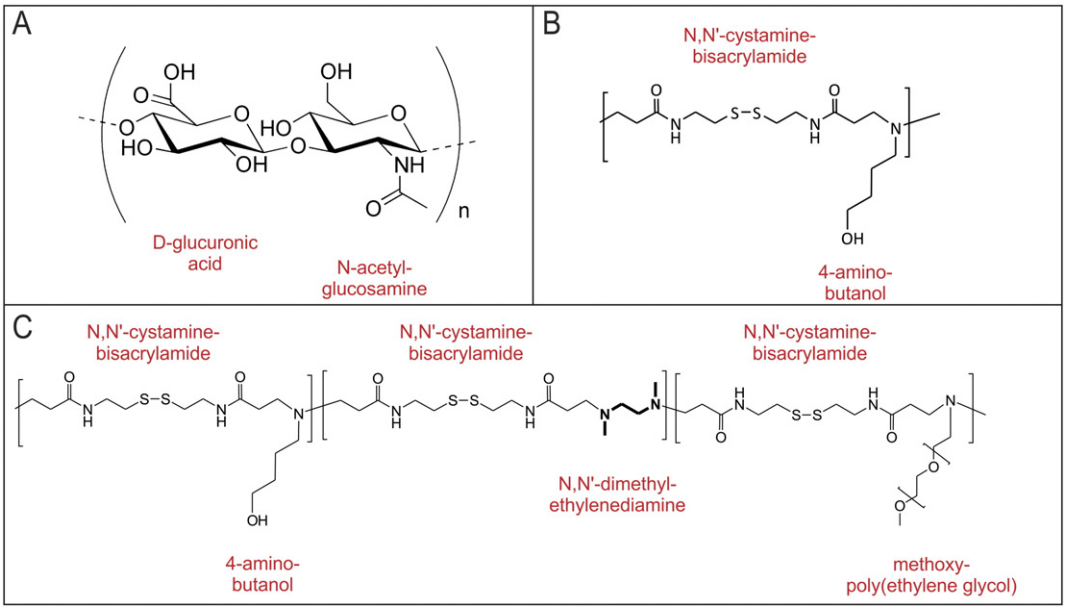

Fig. 2. Chemical structure of (A) hyaluronic acid, (B) p(CBA-ABOL) and (C) p(CBA-ABOL-DMEDA′-PEG).

gene nanomedicines, composed of anionic plasmid DNA and the cationic N,N′-cystaminebisacrylamide-4-aminobutanol (p(CBA-ABOL) vector) (Fig. 2B), have shown promising gene transfection results in vitro with minimal cytotoxicity, owing to the repetitive disulfide linkages in the main poly(amido amine) backbone [9,24]. We demonstrate that electrostatic coating of the cationic polyplexes with HA results in negatively charged nanoparticles without compromising their ability to encapsulate pDNA. Furthermore, by comparing the intravitreal mobility of the nanoparticles in an ex vivo, single-particle based model, we show that coating with HA of 22 kDa and 137 kDa provides a marked increase in the mobile fraction of polyplexes. Finally, this study also documents the ability of these ternary PECs to interact with RPE cells in vitro. With flow cytometry we show that the nanoparticles are still taken up by ARPE-19 cells and are able to induce GFP expression in the target cells, with minimal cytotoxic effects to the cells.

2. Materials and methods

2.1. Materials

Dulbecco's modified Eagle's medium supplemented with growth factor F12 (DMEM:F12 (1:1), OptiMEM™, Trypan Blue, L-glutamine, fetal bovine serum (FBS), penicillin–streptomycin solution (5000 IU/mL penicillin and 5000 μg/mL streptomycin) (P/S), and Dulbecco's phosphate-buffered saline (DPBS 1×, with or without Ca^{2+}/Mg^{2+}) were supplied by GibcoBRL (Merelbeke, Belgium). Sodium hyaluronate of different MWs was purchased from LifeCore Biomedical (Minnesota, USA). All other reagents were purchased from Sigma-Aldrich (Bornem, Belgium) unless otherwise stated.

2.2. Chromatographic analysis of hyaluronic acid

The MWs of HA (Fig. 2A) were determined with a Malvern Viscotek GPCmax (Pump and Injector) and a Malvern Viscotek TDA 302 detector (contains a refractive index, light scattering (RALS and LALS) and viscosity detection). The eluent was PBS (pH = 7.4) at a flow rate of 1 ml/min and 2 Agilent PL aquagel-OH Mixed 8 μm columns were used in series. Columns and detectors were operated at 30 °C. Calibration was done with a pullulan standard (180 kDa) also provided by Malvern. Data were recorded and the molecular weights were calculated with Malvern Omnisec software version 4.7.

2.3. Plasmids

The plasmid constructs pGL4.13 and gwiz-GFP (Promega, Leiden, The Netherlands) were amplified in transformed *E. coli* bacteria and isolated from a bacteria suspension with a Purelink™ HiPure Plasmid DNA Gigaprep kit K2100 (Invitrogen, Merelbeke, Belgium). Concentration and purity were determined by UV absorption at 260 nm and 280 nm on a NanoDrop 2000c (Thermo Fisher Scientific, Rockford, IL, USA). Finally, the plasmids were suspended at a concentration of 1 μg/μl and stored in 25 mM HEPES, pH 7.2, at −20 °C. Fluorescent labeling of pGL4.13 plasmids with YOYO-1™ (λ_{exc} = 491 nm, λ_{em} = 509 nm, Molecular Probes, Merelbeke, Belgium) was performed according to the manufacturer's instructions and as previously published [9]. Briefly, YOYO-1 iodide (1 mM in DMSO) was added to the plasmid at a mixing ratio of 0.15:1 (v:w), resulting in a theoretical labeling density of 1 YOYO-dye molecule per 10 base pairs. The mixture was incubated at room temperature for 4 h in the dark. To remove the DMSO and free YOYO-1, the labeled plasmid was precipitated by adding 2.5 volumes of ice-cold ethanol and 0.1 volumes of 5 M NaCl. After incubation for 30 min at −80 °C, centrifugation (14,600 *g*, 30 min) and washing with clean 70% ethanol, fluorescently labeled plasmid was finally resuspended in 25 mM HEPES, pH 7.2. The concentration of the plasmid was again determined by UV absorption at 260 nm, and adjusted to 1 μg/μl.

2.4. Polyplexes

The polyplexes were made using the bioreducible polymer vector p(CBA-ABOL) (Fig. 2B), which is a linear poly(amido amine) with repetitive disulfide linkages in the main chain, prepared by Michael-type polyaddition of 4-aminobutanol (ABOL) to N,N′-cystaminebisacrylamide (CBA), yielding polymers with an average MW of 5.24 kDa [9,24]. p(CBA-ABOL)/DNA complexes were obtained by adding a polymer solution to a plasmid solution in a final mass ratio of 48/1 in 25 mM HEPES buffer pH 7.2, resulting in an N/P ratio of 45/1. The mixture was vortexed for 10 s, after which they were allowed to stabilize for approximately 15 min at room temperature.

Electrostatic coating of the previously prepared polyplexes was performed by adding HA-solution, with the appropriate amount of HA for the desired molar ratio, to an equal volume of polyplexes and vortexing 10 s, after which the ternary complexes were again allowed to stabilize for 10 min.

For the PEGylated polyplexes, p(CBA-ABOL/DMEDA′/PEG) (Fig. 2C) was used as polymer vector, obtained by Michael-type poly-addition of methoxyPEG amine (2250 Da), N,N′-dimethylethylenediamine (DMEDA′) and ABOL to CBA in a CBA/ABOL/DMEDA′/PEG molar ratio of 50/34/11/5, yielding polymers with an average MW of 7.3 kDa. The same protocol was used for the preparation and characterization of these polyplexes.

Fluorescently labeled polyplexes were obtained by using YOYO1-labeled plasmids, which has been described in the previous section. The plasmid was labeled instead of the vector, to minimize the influence of the labeling on the particle surface characteristics.

2.5. Physical characterization of gene nanomedicines

Hydrodynamic diameter, polydispersity index (PDI) and zeta potential were measured by dynamic light scattering (DLS) with a NanoZS Zetasizer (Malvern Instruments, Hoeilaart, Belgium). All samples were measured in triplicate, diluted in 25 mM HEPES buffer pH 7.2 to evaluate the stability of nanoparticles.

2.6. Gel electrophoresis

Polyplexes were prepared as previously described. Polyplexes (uncoated, HA-coated and PEG-coated) corresponding to 50 ng pDNA were diluted and incubated in HEPES, after which 5 μl of Ambion loading buffer (Ambion, Merelbeke, Belgium) was added to the suspension. The mixtures were loaded into a 1% agarose gel in 1 × TBE buffer, to which GelRed (Biotium, Hayward, CA) was added for visualization of the pDNA. The gel was run for 40 min at 100 V and imaged.

2.7. Cell culture

ARPE-19 cells (retinal pigment epithelial cell line; ATCC number CRL-2302) were cultured in Dulbecco's modified Eagle's medium supplemented with growth factor F12 (DMEM:F12 (1:1), 10% FBS, 2 mM L-glutamine and 50 μg/ml penicillin/streptomycin). Cells were incubated at 37 °C in a humidified atmosphere containing 5% CO2 and subcultured every 3 to 4 days. Cellular experiments were performed on cells in culture with passage number below 20.

2.8. Detection of CD44 expression on ARPE-19 cells by immunohistochemistry

ARPE-19 cells were seeded in T25 cell culture flasks. When reaching +/− 70% confluency, they were detached with non-enzymatic cell dissociation buffer (Sigma-Aldrich, Bornem, Belgium) and counted. 100,000 cells were washed with flow buffer, after which they were incubated for 30 min with a primary anti-CD44 antibody produced in rabbit (Sigma, Bornem, Belgium). After washing, the cells were incubated with a green fluorescent bovine secondary anti-rabbit IgG-FITC antibody (Santa Cruz Biotechnology, Dallas, TX) for 30 min in the dark. After washing, the surface marker expression was evaluated with flow cytometry (FACSCalibur™, BD Biosciences Benelux N.V., Erembodegem, Belgium).

2.9. Uptake and transfection efficiency

ARPE-19 cells were plated in 24 well plates at 45,000 cells/well and allowed to grow overnight. The next day, polyplexes were prepared with YOYO1-labeled pGL4.13 plasmids as described above, added to the cells in serum-free OptiMEM™ at a concentration of 1 μg pDNA/45,000 cells, and incubated for 2 h at 37 °C in an incubator. As a negative control, ARPE-19 cells were pre-incubated on ice for 1 h, and also incubated with the particles on ice. After incubation, the particles were removed and ice-cold Trypan Blue was added to each well to quench extracellular fluorescence from polyplexes attached to the cell membrane. After removal of Trypan Blue, the cells were washed with Dulbecco's phosphate buffered saline (DPBS 1× without Ca^{2+}/Mg^{2+}), trypsinized and centrifuged for 7 min at 300 g, after which they were resuspended in flow buffer (1% bovine serum albumin and 0.1% sodium azide in DPBS). The green fluorescence from the plasmids in the cell interior was measured by flow cytometry (FACSCalibur™, BD Biosciences Benelux N.V., Erembodegem, Belgium).

For transfection experiments, cells were plated similar to the uptake experiments. 1 day after cell seeding, polyplexes were prepared with gwiz-GFP plasmid to measure transfection efficiency and pGL4.13 plasmid as a negative control, since luciferase expression does not produce a detectable fluorescence signal in the GFP-emission spectrum. Incubation of the cells was done similar to the uptake experiments, where 1 μg pDNA was added to each well and incubated for 2 h at 37 °C. Afterwards, the polyplexes were removed, cells were washed with PBS and fresh medium was added for 22 h incubation. 24 h after the particles were added, the cells were trypsinized and GFP expression was examined by flow cytometry.

2.10. Flow cytometry

After inhibition of trypsinization by cell culture medium, cells were centrifuged for 7 min at 300 *g* and supernatant was removed. Cells were resuspended in flow buffer and cell-associated fluorescence was analyzed with a FACSCalibur (Beckton Dickinson, Erembodegem, Belgium) equipped with an Argon laser (excitation 488 nm). For quantification, all experiments were performed in triplicate and for each sample, data were collected for 30 s consisting of side scatter, forward scatter and fluorescence emission of YOYO-1 dye (uptake experiments) or GFP (transfection experiments) with a 530/30 nm bandpass filter (FL1). Cellquest software (Beckton Dickinson, Erembodegem, Belgium) was used for analysis. Appropriate gating was applied to the forward/side-scatterplot of untreated cells to select for intact cells. A cell was considered positive for YOYO-1 or GFP fluorescence, if the average fluorescence was above the threshold T, defined as the 99.5 percentile of the negative control sample.

2.11. Uptake after saturation of HA receptors

ARPE-19 cells were plated in 24 well plates at 45,000 cells/well and allowed to grow overnight. The next day, cells were pre-incubated for 1 h with 2 mg/ml HA-solutions. After 1 hour incubation, polyplexes prepared with YOYO1-labeled pGL4.13 plasmids as described above, were added to the cells at a concentration of 1 μg pDNA/45,000 cells, and incubated for 2 h at 37 °C in an incubator. After incubation, cells were treated and analyzed as described above.

2.12. Cytotoxicity

Cytotoxicity of the polyplexes was evaluated with an MTT assay. ARPE-19 cells were plated in 24 well plates at 45,000 cells per well. Similar to the transfection protocol, pGL4.13-polyplexes, prepared as previously described, were added to the cells in serum-free OptiMEM™ and incubated for 2 h at 37 °C. After removal of the polyplexes, fresh cell culture medium was added to the cells. 24 h after addition of the nanoparticles, MTT reagent was added to full cell culture medium for 4 h at 37 °C. Afterwards, cells were washed and lysed with cell lysis buffer (0.04 N HCl and 1% Triton-X in isopropanol) for 1 h on a shaker. Then, absorbance at 590 nm and 690 nm is measured with a plate spectrophotometer (PerkinElmer 2104 EnVision®), where A_{590} relates to the metabolic activity, and A_{690} is used as a reference wavelength.

2.13. Statistical analysis

Statistical tests were performed in IBM® SPSS® Statistics version 22. Normality of all triplicates was verified with a Shapiro–Wilks test. Average values were further compared by means of independent samples *t*-test or Welch's *t*-test, based on the outcome of the Equality of Variances Levene test. The mean difference was considered significant at the $p < 0.05$ level.

2.14. Fluorescence single particle tracking (fSPT) microscopy

For the diffusion measurements in HEPES buffer (25 mM, pH 7.2), the nanoparticles were diluted to a concentration suitable for fSPT (typical concentrations of 10^8 to 10^{10} particles per ml). 9 μl of these samples was then applied between a microscope slide and a cover glass with a double-sided adhesive sticker of 120 μm thickness in between (Secure-Seal Spacer; Molecular Probes, Leiden, The Netherlands). The microscope was always focused at 5 to 10 μm above the cover glass. For each sample, typically 10 to 20 movies of about 200 frames each were recorded at different locations within the sample, at a frame rate of 24 or 35 fps depending on the exposure time. All fluorescence video imaging of diffusing nanoparticles was performed on a custom-built laser wide field fluorescence microscope setup. Diffusion analysis of the videos was performed off-line using in-house developed software, as described before [25], providing a distribution of apparent diffusion coefficients. For a more detailed description of both the fSPT setup and the trajectory analysis, the reader is referred elsewhere [9].

2.15. Ex vivo evaluation of intravitreal polyplex mobility

Intravitreal mobility of nanoparticles in vitreous humor was evaluated with fSPT microscopy in an ex vivo model as previously described [9]. In short, fresh bovine eyes were obtained from the local slaughterhouse, subsequently disposed of extraocular material and incised along the limbus. Then, the cornea and lens were removed, exposing the anterior part of the hyaloid membrane that holds the vitreous body. This optical "window" was juxtaposed to the glass cover slip of a MatTek glass bottom dish (35 mm, No. 1.5, MatTek Corporation, MA, USA). Finally, to avoid drift of the eye inside the glass bottom dish, the eye was gently fixed with parafilm. For all vitreous experiments, the sclera was punctured laterally with a 21 G guard needle (BD Microlance, BD Biosciences Benelux N.V., Erembodegem, Belgium), after which 10–20 μl of nanoparticle suspension was injected into the vitreous humor with the help of a syringe and 25 G spinal needle (BD Microlance, BD Biosciences Benelux N.V., Erembodegem, Belgium). The nanoparticles were expunged from the syringe near the cover slip to allow visualization within the working distance of the objective lens, though far enough to avoid punctuation of the anterior hyaloid membrane and subsequent outflow of vitreous liquid. Next, the sample was stored for 24 h at room temperature before performing the microscopy experiments, thus allowing the nanoparticles to diffuse from the injection site into the surrounding vitreous and within the working range of the objective lens.

3. Results

3.1. Characterization of hyaluronic acid

HA was purchased with three different MWs of 20 kDa, 200 kDa and >1.8 MDa according to the manufacturer. These samples were analyzed with gel permeation (size exclusion) chromatography, and the measured MWs and dispersity are presented in Table 1. Based on the weight-averaged MW distributions (M_W), we will refer to the different samples as HA22, HA137 and HA2700.

3.2. Physical characterization of CBA-ABOL/pDNA polyplexes

Gene complexes were prepared from CBA-ABOL polymers and pDNA at an N/P ratio of 45/1 according to previously published data [9,24,26], with N and P representing the amine groups in the cationic polymer and phosphate groups in the NAs, respectively. Their hydrodynamic diameter, PDI and surface charge were measured in 25 mM HEPES buffer, pH 7.2 with DLS (Table 2). CBA-ABOL/pDNA polyplexes had a size of +/− 108 nm and a positive zeta potential of +29 mV. Also PEGylated polyplexes were prepared from CBA-ABOL-DMEDA-PEG/pDNA [9,27], resulting in slightly larger particles with a close to neutral surface charge.

Preformed CBA-ABOL/pDNA polyplexes were electrostatically coated with HA at 45/1/100 and 45/1/200 molar N/P/C ratios, where P and C refer to the anionic phosphate groups in the NAs and carboxyl groups of the HA monomers, respectively, and N refers solely to the cationic amine groups present in the polycation. Because for HA2700-coated polyplexes, flocculation of the nanoparticles was visible by the naked eye, the DLS results were excluded from Table 2 due to the inherent limitation of DLS results in the case of sedimentation. To evaluate if pDNA is still retained in the polyplexes after HA coating, gel electrophoresis was performed of HA-coated polyplexes prepared in HEPES buffer. As can be seen from the results in Fig. 3, HA coating did not displace pDNA from the polyplexes. Only for the PEGylated polyplexes, a fraction of pDNA was not complexed, as apparent by the fluorescent smear from the well. In conclusion, electrostatic coating of CBA-ABOL/pDNA polyplexes with HA can result in stable gene nanomedicines with negative surface charge, which are still able to retain their pDNA cargo. In order to compare between different MWs of HA coating, the N/P/C ratio should be kept constant. Therefore, we decided using the 45/1/200 ratio for all following experiments, seeing as HA22-coated polyplexes only stabilized around this ratio.

3.3. Intravitreal mobility of HA-coated polyplexes

In a next step we wanted to verify the crucial requirement that HA-coated polyplexes should be mobile in vitreous humor. Therefore, we injected the different nanoparticles in a recently optimized ex vivo model of intact bovine vitreous and visualized the movement of these nanoparticles with fSPT microscopy. Examples of such movies can be found on the online version as supplementary information for uncoated (Supplementary Movie 1), HA22-coated (Supplementary Movie 2), HA137-coated (Supplementary Movie 3) and HA2700-coated

Table 1
MW characterization of the different HA samples by gel permeation chromatography. Shown are the number-averaged (M_n), peak-value (M_p), weight-averaged (M_w) and z-averaged (M_z) MWs of the different fractions in kDa, as well as the dispersity.

	M_n (kDa)	M_p (kDa)	M_w (kDa)	M_z (kDa)	Dispersity (M_w/M_n)
LifeCore 20 kDa	14.86 ± 0.27	19.57 ± 0.12	22.64 ± 0.14	33.33 ± 0.41	1.52
LifeCore 200 kDa	88.9 ± 7.7	126.7 ± 1.1	136.9 ± 3.3	213 ± 11	1.54
LifeCore >1.8 MDa	2606 ± 11	2510 ± 340	2764 ± 25	3038 ± 36	1.06

Table 2
Size, PDI and zeta potential of polyplexes in HEPES buffer, as measured by dynamic light scattering.

	25 mM HEPES buffer, pH 7.2		
	Z-averaged diameter (nm)	PDI	Zeta potential (mV)
CBA-ABOL/pDNA	108 ± 3	0.134 ± 0.054	29 ± 3
CBA-ABOL-DMEDA-PEG/pDNA	124 ± 5	0.381 ± 0.034	10 ± 1
HA22-pplxs 45/1/100	1820 ± 150	0.878 ± 0.062	−20 ± 1
HA22-pplxs 45/1/200	647 ± 19	0.401 ± 0.044	−22 ± 1
HA137-pplxs 45/1/100	312 ± 2	0.209 ± 0.015	−26.6 ± 0.1
HA137-pplxs 45/1/200	343 ± 4	0.214 ± 0.016	−29.9 ± 0.5
HA2700-pplxs 45/1/100[a]	/	/	−28 ± 2
HA2700-pplxs 45/1/200[a]	/	/	−37 ± 2

PDI: polydispersity index; pplxs: polyplexes.
[a] Clearly-observed flocculation during particle preparation in HEPES buffer.

(Supplementary Movie 4) polyplexes. The diffusion coefficients were determined for individual polyplexes from their motion trajectories, the results of which are combined in a distribution and presented in Fig. 4. The black line represents the distribution of diffusion coefficients of uncoated p(CBA-ABOL)/pDNA polyplexes in vitreous humor, showing a bimodal distribution with the majority of polyplexes being immobilized, similar to what we observed before [9]. We hypothesize that the small mobile fraction of the nanoparticle population is a consequence of spontaneous electrostatic coating of native HA on the cationic polyplexes. The mobility of HA137-coated polyplexes is improved the most (solid purple line), followed by HA22 coated polyplexes (solid red line). Interestingly, the mobile fractions of HA22-and HA137-coated polyplexes show distributions of diffusion coefficients that are nearing those obtained in pure buffer solution, indicating close to maximum diffusional mobility within the vitreous body. HA2700-coated polyplexes, on the other hand, did not show any improvement. This is presumably due to the large size and aggregation of HA2700-coated polyplexes in buffer. Though this is not evident from DLS data (Table 2), during preparation of the ternary PECs, flocculation of the nanoparticles was visually observed when high concentrations of high molecular weight HA (HMWHA) was added to the cationic polyplexes, presumably as a result of their high viscosity (Supplementary Fig. 1 and Supplementary Table 1). Alternatively, it could be hypothesized that the complete complexation of HMW HA to the polyplex surface would lead to a substantial loss of conformational entropy. Therefore, it seems likely that the HA chains only slightly bind to the polyplex and for the most part remain in their coiled form, leaving other binding sites available for binding to other particles and resulting in aggregation.

3.4. Uptake, transfection and cytotoxicity of HA-coated polyplexes in RPE cells

Following the observation that coating with HA22 or HA137 ensures good mobility of polyplexes in vitreous humor, we have evaluated if these HA-polyplexes can still transfect RPE cells. Seeing as electrostatic coating of p(CBA-ABOL)/pDNA polyplexes with HA2700 does not further improve intravitreal mobility, we have excluded these particles in the following experiments. The results of cell uptake and transfection efficiencies quantified by flow cytometry are shown in Fig. 5. Clearly, PEGylation of the polyplexes results in a lack of cell uptake (Fig. 5A–B) and, therefore, GFP expression (Fig. 5C–D). On the other hand, both HA22-and HA137-coated polyplexes were taken up in close to 100% of the cells, most likely due to receptor mediated endocytosis (Fig. 5A). Nevertheless, whereas HA22-coating appears to result in more or less similar uptake to non-functionalized polyplexes, HA137-coated polyplexes clearly show a lesser overall uptake efficiency when looking at uptake on a per-cell basis (Fig. 5B). Looking at the efficiency of GFP expression, both HA-coated polyplexes were able to transfect the RPE cells (Fig. 5C–D), though not as efficiently as non-functionalized polyplexes, and again transfection efficiencies of HA137-coated polyplexes were seemingly lower than HA22-coated polyplexes.

We additionally tested the toxicity of the different types of polyplexes by measuring the metabolic activity of cell populations with an MTT assay. The values shown in Fig. 5E are normalized against untreated ARPE-19 cells. No cytotoxicity was observed for any of the polyplexes at the same concentrations employed for the uptake and transfection

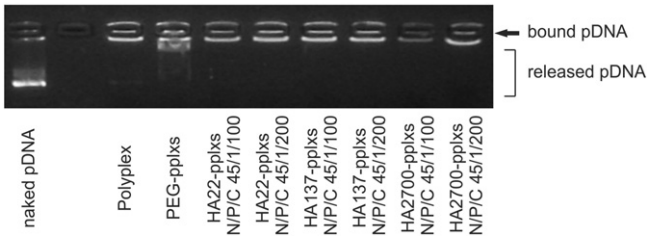

Fig. 3. pDNA complexation efficiency of polyplexes. Gel electrophoresis shows successful pDNA complexation of the different polyplexes in HEPES. Only the PEGylated polyplexes show some pDNA displacement, seen as a smear in the gel, though the majority of pDNA remains complexed, as evident from the fluorescence in the wells.

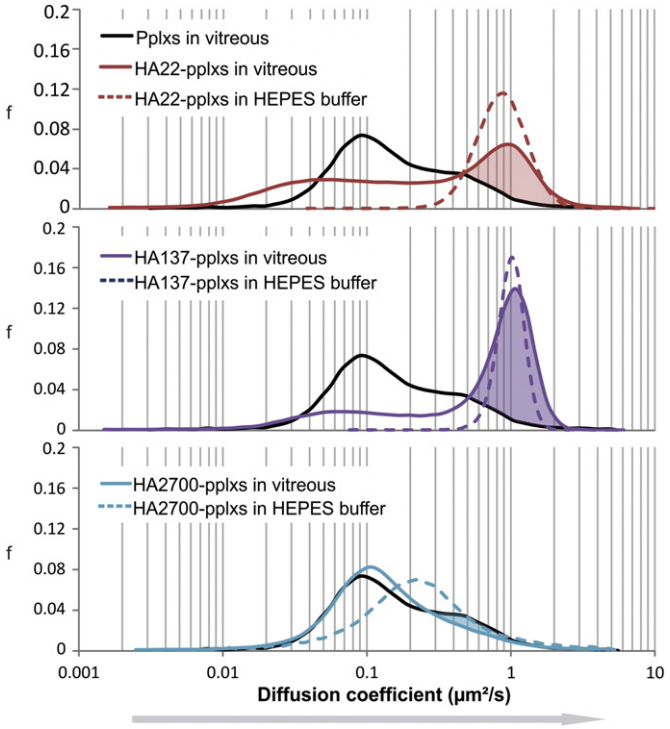

Fig. 4. Single particle tracking analysis of the intravitreal mobility of HA-coated polyplexes. A bimodal distribution of diffusion coefficients can be seen for the uncoated, cationic polyplexes in vitreous humor (black, solid line). The highest increase in mobility was found for HA137-coated polyplexes, while no improvement was found for HA2700-coated polyplexes. The mobility of the respective HA-coated nanoparticles in HEPES buffer is also shown as a reference (dotted lines).

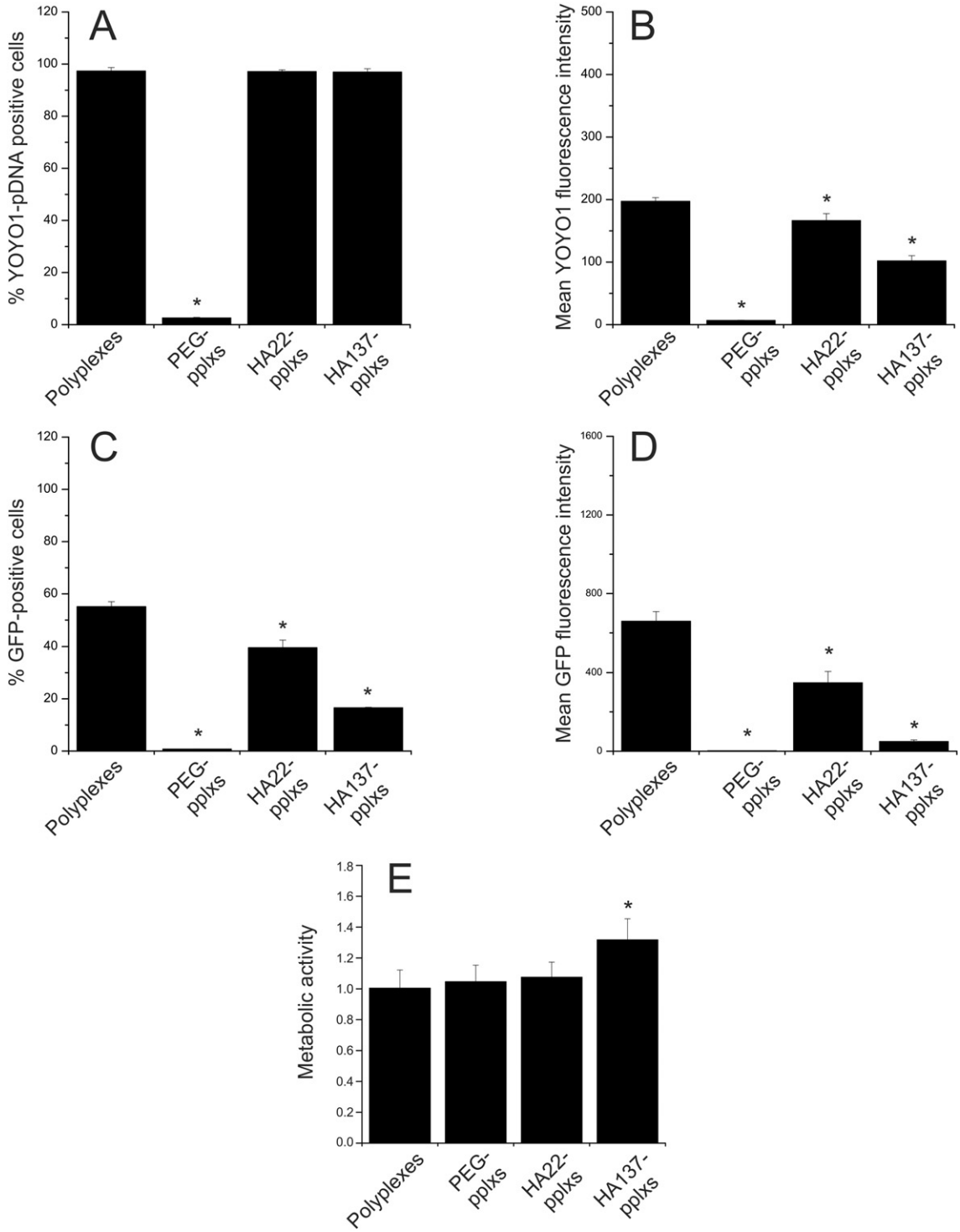

Fig. 5. Uptake, transfection and cytotoxicity of HA-coated polyplexes in ARPE-19 cells. (A) Percentage of ARPE-19 cells which are positive for YOYO-1-labeled polyplexes, evaluated by flow cytometry. (B) Mean YOYO-1 fluorescence intensity of the ARPE-19 cell population, evaluated by flow cytometry. (C) Percentage of ARPE-19 cells that are positive for GFP fluorescence. (D) Mean GFP fluorescence intensity of the ARPE-19 cell population, evaluated by flow cytometry.(E) Metabolic activity of ARPE-19 cell population after treatment with different polyplexes, measured by MTT assay and normalized against untreated cells. All values are the mean of 3 repetitions and the error bars represent the standard deviation. (*) $p < 0.05$ with respect to non-functionalized polyplexes (independent samples t-test).

experiments. It can even be seen that the HA137-coating results in the cells being metabolically more active than the untreated cell population.

3.5. Involvement of CD44-receptor in uptake of HA-coated polyplexes

Since the HA-coated particles are taken up despite their negative charge, it is likely that they are internalized through ligand-receptor interactions. As HA is a well-known ligand for the CD44-receptor, we verified CD44-expression on the surface of ARPE-19 cells. This was confirmed by means of antibody-based surface marker expression analysis via flow cytometry (Fig. 6A). To further verify the involvement of this receptor in HA-polyplex uptake, we pre-incubated the cells with HA of the respective MW in order to saturate the CD44 receptors and prevent interaction with HA-coated polyplexes. As shown in Fig. 6B, a statistically

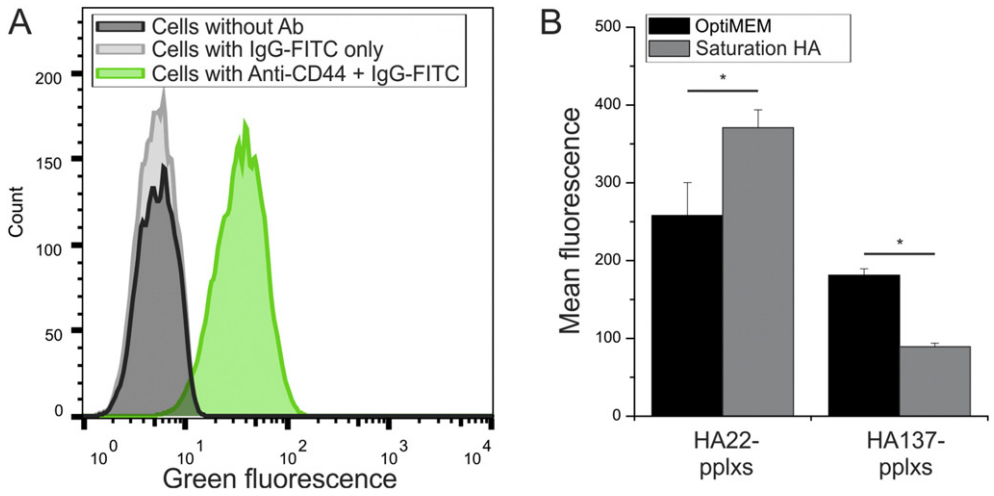

Fig. 6. CD44-mediated endocytosis of polyplexes. (A) CD44-expression on ARPE-19 cells is verified by flow cytometry (green curve). A representative distribution is shown selected from three replicates. (B) The influence on the cellular uptake of HA-coated polyplexes after saturation of the CD44 receptors with HA of the same MW. (*) Mean difference is significant at $p < 0.05$ level (independent samples t-test).

significant decrease in polyplex uptake was seen in case of HA137-coating. Surprisingly, saturation of ARPE-19 cells with HA22 resulted in a statistically significant increase in uptake of HA22-coated polyplexes.

4. Discussion

Intravitreal injection is generally regarded as a promising administration route for larger MW therapeutics or nanomedicines intended for retinal delivery, as it bypasses most of the natural barriers of the eyes. Nonetheless, the mobility of these therapeutics in the vitreous humor is of utmost importance in order to reach the retinal target cells. Indeed, we have previously reported that surface characteristics such as hydrophobicity and cationic charge can be detrimental for intravitreal mobility, inducing aggregation and immobilization of the nanomedicines in the vitreal matrix [9]. The vitreous humor is composed of a random network of collagen-fibrils interspersed with anionic glycosaminoglycans, most notably HA, stabilizing the network by ensuring hydration and inflation of the collagen fibrils [20]. Due to the anionic nature of the vitreous humor, immobilization of cationic nanoparticles is to be expected [9,10]. Though PEGylation was previously shown to improve nanomedicine mobility [9], it almost completely inhibits cell uptake and transfection, as shown in Fig. 5. We hypothesized that HA could be a suitable alternative for PEG, due to the fact that it is one of the major constituents of the vitreous humor and that it is a ligand to the CD44 receptor, which is expressed in RPE [22] and other retinal cells [23]. Due to its ubiquitous and biocompatible nature, HA has also been frequently employed as a surface coating for nanomedicines in cancer therapy, acting as a natural stealth molecule and targeting ligand of CD44-overexpressing tumor-tissues [15,16,28,29]. HA is known to regulate a multitude of different cascades and processes in mammalian organisms, which are thought to be dependent on the MW of the HA chains [30,31]. In other words, the MW of HA influences its biological function and possibly the affinity towards the CD44-receptor and other hyaladherins. This aspect has remained overlooked in the majority of the literature concerning the use of HA as an additive in drug delivery vectors, resulting in contradictory findings being published [13].

In our study, HA of different MWs was electrostatically coated on preformed binary PECs composed of anionic pDNA and cationic p(CBA-ABOL) polymers. A similar approach was previously reported for low molecular weight HA (LMWHA) and polyethylenimine (PEI)-polyplexes in the context of tumor-targeting and corneal gene therapy, respectively [32,33]. Our method provided stable nanoparticles with a negative surface charge, which maintained efficient complexation of pDNA (Table 2 and Fig. 3). An approximately 4-fold higher molar ratio of HA negative charges compared to polymer positive charges was necessary to stabilize the nanoparticles, resulting in a molar N/P/C ratio of 45/1/200. As the nanoparticles are formed by spontaneous complexation of cationic polymers and anionic pDNA, it is expected that a certain amount of free polymer will always be present in the solution and could be argued that HA will form complexes with these free polymer molecules. Though gel electrophoresis experiments proved that pDNA is still complexed by the polyplexes, it would be interesting to focus future research on a covalent attachment of HA to the nanoparticle or polyplex surface. Interestingly, electrostatic coating with HA137 appeared to require a lower amount of HA to provide stable complexes than HA22 or HA2700. Furthermore, it was noticed that electrostatic coating with HA2700 resulted in heavy flocculation of the gene nanomedicines. This can be attributed to the high viscosity of the suspension due to the high concentration of HA at 45/1/200 molar N/P/C ratio (Supplementary Fig. 1 and Supplementary Table 1), or alternatively to the HMW HA remaining for the most part in an entropically favored coiled state, leaving several HA-binding sites available for bridging of adjacent polyplexes.

Next we have evaluated the effect of coating cationic polyplexes with HA of various MWs on their mobility in the vitreous humor. For this we used our previously optimized ex vivo vitreal model that allows to observe and analyze the mobility of the polyplexes by fSPT microscopy [9]. By analyzing the mobility of many individual polyplexes, potential heterogeneity of the population can be readily exposed. As before [9], a bimodal distribution was found for uncoated cationic polyplexes indicating that a large fraction is immobilized, likely by binding to collagen fibrils (Fig. 4). By electrostatic coating of the polyplexes with HA of various MWs, a clear improvement in mobility was observed. Coating with HA137 resulted in the highest increase in fraction of mobile nanoparticles, followed by HA of 22 kDa. The smaller size of HA137-polyplexes should not be used as an explanation for this increase fraction of mobile nanoparticles, since in our previous study we have found that (PEGylated) nanoparticles up to 1 μm can diffuse freely through the vitreous humor [9]. The fact that a small fraction of HA-coated polyplexes remains immobilized could indicate that the electrostatic coating is not perfect for all particles in the population. Especially for this type of polyplexes, where an excess of cationic polymer is added and free polymer might be available around the nanoparticles, it can be contended that the physical properties of PECs are influenced depending on their surrounding biological matrix or environment. For example, we have seen before that nanoparticle diffusion in bovine vitreous should be slowed down by a factor of 2 compared to diffusion in HEPES buffer [9]. However, in Fig. 4 we observe almost no difference in diffusion coefficient

between HA-coated nanoparticles in HEPES buffer and those HA-coated nanoparticles that remain mobile in the vitreous humor. We suggest this is attributed to a reorganization of the ternary PECs in the vitreous humor due to the presence of several charged vitreal components, resulting in a decreased size and therefore higher diffusion coefficient in vitreous humor. As previously stated, in future research it would be interesting to evaluate a covalently attached HA-coating instead, or a coating of predefined gene nanomedicines. In any case, our findings are in line with recent in vivo reports where self-assembled amphiphilic polymeric nanoparticles (composed of a conjugate of HA and 5β-cholanic acid) and HA-modified core-shell liponanoparticles (composed of a chitosan core and cholesterol:DOPE) were found in the retina after intravitreal injection in rats, indicating intravitreal mobility of nanoparticles with an HA-coated surface [34,35].

Apart from mobility in the vitreous humor, it is of equal importance that the polyplexes are capable of transfecting the target cells. Recently, uptake of HA-coated solid lipid nanoparticles in the ARPE-19 cell line was reported, although the particles used in that study still had a cationic surface charge [36]. In our study, cationic polyplexes were coated with HA until a negative surface charge was obtained as we have previously found that cationic particles are immobile in the vitreous body. We found that, despite their negative surface charge, our HA-coated polyplexes are still capable of being taken up by the ARPE-19 cells and induce transfection (Fig. 5) without noticeable cytotoxicity. Likely this uptake is mediated by interaction with CD44-receptors, which we showed to be present on the cell surface (Fig. 6A). HA22-coated polyplexes were highly efficient at transfecting ARPE-19 cells, almost to the same extent as uncoated polyplexes (Fig. 5C), while HA137-coating resulted in less GFP expression. These differences were in line with the extent of polyplex uptake (Fig. 5B). The lower transfection efficiency of HA137-coated polyplexes might additionally be due to increased cell proliferation, resulting in dilution of the transgene over a larger population of cells (Fig. 5E). Indeed, we noticed that incubating ARPE-19 cells with HA137-coated polyplexes for 2 h resulted in an increased metabolic activity 22 h later. This can be related to previously published findings which indicate that LMWHA (20–500 kDa) is pro-angiogenic and stimulates proliferation of vascular smooth muscle cells, whereas HMWHA (several million Da) is thought to have the opposite effect [37–39]. Indeed, Ferguson et al. [31] also documented a slight, though not statistically significant, increase in cell viability when normal fibroblasts were incubated with HA fragments of 120–360 kDa. A possible explanation for this increase in metabolic activity was postulated by Grishko and colleagues [40], who indeed noticed that free HA in the 500 kDa range typically increased mitochondrial reductase activity in chondrocyte primary cultures.

Nevertheless, based on previously published studies trying to elucidate the optimal MW for interactions with CD44-receptors [41,42] and uptake by CD44-expressing cells [15,29,35], we expected that HA137-coated polyplexes would be taken up more efficiently than HA22-coated nanoparticles. It is generally accepted that HMWHA leads to better uptake of HA-nanoparticles, presumably because it provides more multivalent interactions with the CD44-receptor [15,41]. The differences between our results and previously published research might be due to differences in CD44-receptor characteristics. Indeed, uptake and interactions were compared in different cell types, which could mean different CD44-receptor density, clustering and turn-over rate, leading to differences in interactions with HA-ligands. Interesting to note is a recent study by Almalik et al. [43], where it is hypothesized that a slow turn-over rate of CD44-receptors in RAW264.7 cells is the rate-limiting step for HA-nanoparticle uptake. However, a higher presentation of HA would result in a higher affinity to the CD44-receptor and therefore limit capacity/uptake rate of HA-coated nanoparticles. To investigate involvement of hyaladherins in HA-polyplex uptake, we also performed a competitive binding assay with free HA (Fig. 6B), where cells were pre-incubated with free HA before addition of HA-coated nanoparticles. Interestingly, saturation of hyaladherins with HA137 significantly affects uptake of HA137-coated polyplexes, whereas a reversed effect was noticed for HA22-polyplexes. This could indicate that indeed, HA137 has a higher affinity for the hyaladherins, CD44 and others, present on the ARPE-19 cells and therefore free HA137 inhibits uptake of the HA-coated polyplexes. Likewise, HA22 has a much lower affinity for these hyaladherins, which could be why the uptake of HA22-coated particles is not diminished by free HA.

5. Conclusion

We present here an easy way of modifying cationic gene nanomedicines with HA for improved retinal drug delivery efficacy after intravitreal administration. Electrostatic coating of polyplexes with HA results in ternary gene polyplexes with an anionic, hydrophilic shell. The high viscosities inherent to high concentrations of HA2700, impeded the stabilization of HA2700-coated polyplexes. Using HA22 and HA137 however, immobilization of therapeutics in the vitreal network is prevented. Furthermore, despite their negative charge, the HA-coated polyplexes are still taken up in vitro by retinal target cells, in this case ARPE-19 cells, presumably via CD44-mediated endocytosis. Together, these results demonstrate for the first time that using LMWHA as an electrostatic coating for cationic binary PECs is an easy, biocompatible way to enhance the efficiency of gene nanomedicines to the retina via intravitreal administration.

Supplementary data to this article can be found online at http://dx.doi.org/10.1016/j.jconrel.2015.01.030.

Acknowledgments

This work was supported by a grant from the Brailleliga and Funds for Research in Ophthalmology (FRO), Belgium (http://www.fro-online.org/). Financial support by the Ghent University Special Research Fund (01B04912 and DEF08/FOP/010) and the Fund for Scientific Research Flanders (FWO, Belgium; G019711N) is acknowledged with gratitude. KR is a post-doctoral fellow of the FWO. The authors have no other relevant affiliations or financial involvement with any organization or entity with a financial interest in or financial conflict with the subject matter or materials discussed in the manuscript apart from those disclosed. No writing assistance was utilized in the production of this manuscript.

References

[1] A.M. Maguire, K.A. High, A. Auricchio, J.F. Wright, E.A. Pierce, F. Testa, F. Mingozzi, J.L. Bennicelli, G.S. Ying, S. Rossi, A. Fulton, K.A. Marshall, S. Banfi, D.C. Chung, J.I. Morgan, B. Hauck, O. Zelenaia, X. Zhu, L. Raffini, F. Coppieters, E. De Baere, K.S. Shindler, N.J. Volpe, E.M. Surace, C. Acerra, A. Lyubarsky, T.M. Redmond, E. Stone, J. Sun, J.W. McDonnell, B.P. Leroy, F. Simonelli, J. Bennett, Age-dependent effects of RPE65 gene therapy for Leber's congenital amaurosis: a phase 1 dose-escalation trial, Lancet 374 (2009) 1597–1605.

[2] A.M. Maguire, F. Simonelli, E.A. Pierce, E.N. Pugh Jr., F. Mingozzi, J. Bennicelli, S. Banfi, K.A. Marshall, F. Testa, E.M. Surace, S. Rossi, A. Lyubarsky, V.R. Arruda, B. Konkle, E. Stone, J. Sun, J. Jacobs, L. Dell'Osso, R. Hertle, J.X. Ma, T.M. Redmond, X. Zhu, B. Hauck, O. Zelenaia, K.S. Shindler, M.G. Maguire, J.F. Wright, N.J. Volpe, J.W. McDonnell, A. Auricchio, K.A. High, J. Bennett, Safety and efficacy of gene transfer for Leber's congenital amaurosis, N. Engl. J. Med. 358 (2008) 2240–2248.

[3] S.G. Jacobson, A.V. Cideciyan, R. Ratnakaram, E. Heon, S.B. Schwartz, A.J. Roman, M.C. Peden, T.S. Aleman, S.L. Boye, A. Sumaroka, T.J. Conlon, R. Calcedo, J.J. Pang, K.E. Erger, M.B. Olivares, C.L. Mullins, M. Swider, S. Kaushal, W.J. Feuer, A. Iannaccone, G.A. Fishman, E.M. Stone, B.J. Byrne, W.W. Hauswirth, Gene therapy for leber congenital amaurosis caused by RPE65 mutations: safety and efficacy in 15 children and adults followed up to 3 years, Arch. Ophthalmol.-Chic 130 (2012) 9–24.

[4] A.V. Cideciyan, S.G. Jacobson, W.A. Beltran, A. Sumaroka, M. Swider, S. Iwabe, A.J. Roman, M.B. Olivares, S.B. Schwartz, A.M. Komaromy, W.W. Hauswirth, G.D. Aguirre, Human retinal gene therapy for Leber congenital amaurosis shows advancing retinal degeneration despite enduring visual improvement, Proc. Natl. Acad. Sci. U. S. A. 110 (2013) E517–525.

[5] D.M. Lipinski, M. Thake, R.E. Maclaren, Clinical applications of retinal gene therapy, Prog. Retin. Eye Res. (2012).

[6] P. Charbel Issa, R.E. MacLaren, Non-viral retinal gene therapy: a review, Clin. Exp. Ophthalmol. 40 (2012) 39–47.

[7] K. Remaut, N.N. Sanders, B.G. De Geest, K. Braeckmans, J. Demeester, S.C. De Smedt, Nucleic acid delivery: where material sciences and bio-sciences meet, Mater. Sci. Eng. R 58 (2007) 117–161.
[8] T.R. Thrimawithana, S. Young, C.R. Bunt, C. Green, R.G. Alany, Drug delivery to the posterior segment of the eye, Drug Discov. Today 16 (2011) 270–277.
[9] T.F. Martens, D. Vercauteren, K. Forier, H. Deschout, K. Remaut, R. Paesen, M. Ameloot, J.F. Engbersen, J. Demeester, S.C. De Smedt, K. Braeckmans, Measuring the intravitreal mobility of nanomedicines with single-particle tracking microscopy, Nanomedicine (Lond.) 8 (2013) 1955–1968.
[10] L. Peeters, N.N. Sanders, K. Braeckmans, K. Boussery, J.V. de Voorde, S.C. De Smedt, J. Demeester, Vitreous: a barrier to nonviral ocular gene therapy, Invest. Ophthalmol. Vis. Sci. 46 (2005) 3553–3561.
[11] S. Mishra, P. Webster, M.E. Davis, PEGylation significantly affects cellular uptake and intracellular trafficking of non-viral gene delivery particles, Eur. J. Cell Biol. 83 (2004) 97–111.
[12] N.N. Sanders, L. Peeters, I. Lentacker, J. Demeester, S.C. De Smedt, Wanted and unwanted properties of surface PEGylated nucleic acid nanoparticles in ocular gene transfer, J. Control. Release 122 (2007) 226–235.
[13] K. Raemdonck, T.F. Martens, K. Braeckmans, J. Demeester, S.C. De Smedt, Polysaccharide-based nucleic acid nanoformulations, Adv. Drug Deliv. Rev. 65 (2013) 1123–1147.
[14] D. Peer, A. Florentin, R. Margalit, Hyaluronan is a key component in cryoprotection and formulation of targeted unilamellar liposomes, Biochim. Biophys. Acta 1612 (2003) 76–82.
[15] S. Mizrahy, S.R. Raz, M. Hasgaard, H. Liu, N. Soffer-Tsur, K. Cohen, R. Dvash, D. Landsman-Milo, M.G. Bremer, S.M. Moghimi, D. Peer, Hyaluronan-coated nanoparticles: the influence of the molecular weight on CD44-hyaluronan interactions and on the immune response, J. Control. Release 156 (2011) 231–238.
[16] A. Dufay Wojcicki, H. Hillaireau, T.L. Nascimento, S. Arpicco, M. Taverna, S. Ribes, M. Bourge, V. Nicolas, A. Bochot, C. Vauthier, N. Tsapis, E. Fattal, Hyaluronic acid-bearing lipoplexes: physico-chemical characterization and in vitro targeting of the CD44 receptor, J. Control. Release 162 (2012) 545–552.
[17] C. Surace, S. Arpicco, A. Dufay-Wojcicki, V. Marsaud, C. Bouclier, D. Clay, L. Cattel, J.M. Renoir, E. Fattal, Lipoplexes targeting the CD44 hyaluronic acid receptor for efficient transfection of breast cancer cells, Mol. Pharm. 6 (2009) 1062–1073.
[18] S. Taetz, A. Bochot, C. Surace, S. Arpicco, J.M. Renoir, U.F. Schaefer, V. Marsaud, S. Kerdine-Roemer, C.M. Lehr, E. Fattal, Hyaluronic acid-modified DOTAP/DOPE liposomes for the targeted delivery of anti-telomerase siRNA to CD44-expressing lung cancer cells, Oligonucleotides 19 (2009) 103–116.
[19] D.A. Ossipov, Nanostructured hyaluronic acid-based materials for active delivery to cancer, Expert Opin. Drug Deliv. 7 (2010) 681–703.
[20] P.N. Bishop, Structural macromolecules and supramolecular organisation of the vitreous gel, Prog. Retin. Eye Res. 19 (2000) 323–344.
[21] S.J. Clark, T.D. Keenan, H.L. Fielder, L.J. Collinson, R.J. Holley, C.L. Merry, T.H. van Kuppevelt, A.J. Day, P.N. Bishop, Mapping the differential distribution of glycosaminoglycans in the adult human retina, choroid, and sclera, Invest. Ophthalmol. Vis. Sci. 52 (2011) 6511–6521.
[22] N.P. Liu, W.L. Roberts, L.P. Hale, M.C. Levesque, D.D. Patel, C.L. Lu, G.J. Jaffe, Expression of CD44 and variant isoforms in cultured human retinal pigment epithelial cells, Invest. Ophthalmol. Vis. Sci. 38 (1997) 2027–2037.
[23] T. Shinoe, H. Kuribayashi, H. Saya, M. Seiki, H. Aburatani, S. Watanabe, Identification of CD44 as a cell surface marker for Muller glia precursor cells, J. Neurochem. 115 (2010) 1633–1642.
[24] C. Lin, Z.Y. Zhong, M.C. Lok, X.L. Jiang, W.E. Hennink, J. Feijen, J.F.J. Engbersen, Novel bioreducible poly(amido amine)s for highly efficient gene delivery, Bioconjug. Chem. 18 (2007) 138–145.
[25] K. Braeckmans, D. Vercauteren, J. Demeester, S.C. de Smed, Single particle tracking, in: A. Diaspro (Ed.), Nanoscopy and Multidimensional Optical Fluorescence Microscopy, Taylor and Francis, New York, 2010, pp. 5-1–5-17.
[26] D. Vercauteren, M. Piest, L.J. van der Aa, M. Al Soraj, A.T. Jones, J.F. Engbersen, S.C. De Smedt, K. Braeckmans, Flotillin-dependent endocytosis and a phagocytosis-like mechanism for cellular internalization of disulfide-based poly(amido amine)/DNA polyplexes, Biomaterials 32 (2011) 3072–3084.
[27] C. Lin, J.F.J. Engbersen, PEGylated bioreducible poly(amido amine)s for non-viral gene delivery, Mater. Sci. Eng. C Mater. 31 (2011) 1330–1337.
[28] S. Arpicco, G. De Rosa, E. Fattal, Lipid-based nanovectors for targeting of CD44-overexpressing tumor cells, J. Drug Deliv. 2013 (2013) 860780.
[29] H.S. Qhattal, X. Liu, Characterization of CD44-mediated cancer cell uptake and intracellular distribution of hyaluronan-grafted liposomes, Mol. Pharm. 8 (2011) 1233–1246.
[30] R. Stern, A.A. Asari, K.N. Sugahara, Hyaluronan fragments: an information-rich system, Eur. J. Cell Biol. 85 (2006) 699–715.
[31] E.L. Ferguson, J.L. Roberts, R. Moseley, P.C. Griffiths, D.W. Thomas, Evaluation of the physical and biological properties of hyaluronan and hyaluronan fragments, Int. J. Pharm. 420 (2011) 84–92.
[32] Y. Wang, Z. Xu, R. Zhang, W. Li, L. Yang, Q. Hu, A facile approach to construct hyaluronic acid shielding polyplexes with improved stability and reduced cytotoxicity, Colloids Surf. B: Biointerfaces 84 (2011) 259–266.
[33] M. Hornof, M. de la Fuente, M. Hallikainen, R.H. Tammi, A. Urtti, Low molecular weight hyaluronan shielding of DNA/PEI polyplexes facilitates CD44 receptor mediated uptake in human corneal epithelial cells, J. Gene Med. 10 (2008) 70–80.
[34] H. Koo, H. Moon, H. Han, J.H. Na, M.S. Huh, J.H. Park, S.J. Woo, K.H. Park, I.C. Kwon, K. Kim, H. Kim, The movement of self-assembled amphiphilic polymeric nanoparticles in the vitreous and retina after intravitreal injection, Biomaterials 33 (2012) 3485–3493.
[35] L. Gan, J. Wang, Y. Zhao, D. Chen, C. Zhu, J. Liu, Y. Gan, Hyaluronan-modified core-shell liponanoparticles targeting CD44-positive retinal pigment epithelium cells via intravitreal injection, Biomaterials 34 (2013) 5978–5987.
[36] P.S. Apaolaza, D. Delgado, A.D. Pozo-Rodriguez, A.R. Gascon, M.A. Solinis, A novel gene therapy vector based on hyaluronic acid and solid lipid nanoparticles for ocular diseases, Int. J. Pharm. (2014).
[37] D. Kothapalli, J. Flowers, T. Xu, E. Pure, R.K. Assoian, Differential activation of ERK and Rac mediates the proliferative and anti-proliferative effects of hyaluronan and CD44, J. Biol. Chem. 283 (2008) 31823–31829.
[38] R. Deed, P. Rooney, P. Kumar, J.D. Norton, J. Smith, A.J. Freemont, S. Kumar, Early-response gene signalling is induced by angiogenic oligosaccharides of hyaluronan in endothelial cells. Inhibition by non-angiogenic, high-molecular-weight hyaluronan, Int. J. Cancer 71 (1997) 251–256.
[39] F. Gao, C.X. Yang, W. Mo, Y.W. Liu, Y.Q. He, Hyaluronan oligosaccharides are potential stimulators to angiogenesis via RHAMM mediated signal pathway in wound healing, Clin. Invest. Med. 31 (2008) E106–116.
[40] V. Grishko, M. Xu, R. Ho, A. Mates, S. Watson, J.T. Kim, G.L. Wilson, A.W.t. Pearsall, Effects of hyaluronic acid on mitochondrial function and mitochondria-driven apoptosis following oxidative stress in human chondrocytes, J. Biol. Chem. 284 (2009) 9132–9139.
[41] P.M. Wolny, S. Banerji, C. Gounou, A.R. Brisson, A.J. Day, D.G. Jackson, R.P. Richter, Analysis of CD44-hyaluronan interactions in an artificial membrane system: insights into the distinct binding properties of high and low molecular weight hyaluronan, J. Biol. Chem. 285 (2010) 30170–30180.
[42] J. Lesley, V.C. Hascall, M. Tammi, R. Hyman, Hyaluronan binding by cell surface CD44, J. Biol. Chem. 275 (2000) 26967–26975.
[43] A. Almalik, S. Karimi, S. Ouasti, R. Donno, C. Wandrey, P.J. Day, N. Tirelli, Hyaluronic acid (HA) presentation as a tool to modulate and control the receptor-mediated uptake of HA-coated nanoparticles, Biomaterials 34 (2013) 5369–5380.